RECENT PROGRESS IN DESIGN STUDIES FOR TOKAMAK DEMONSTRATION AND COMMERCIAL POWER PLANTS*

M.A. ABDOU, C.C. BAKER, J. BROOKS,
D. EHST, R. MATTAS, D.L. SMITH
Argonne National Laboratory,
Argonne, Illinois,
United States of America

Abstract

This paper presents a summary of the results of two major tokamak design studies: a commercial power reactor study (STARFIRE) completed recently and a Demonstration Power Plant (DEMO) study presently in progress. Both studies involved participation of national laboratories, industry, and utilities.

Great incentives were identified for developing the option of steady-state plasma operation in tokamaks. A number of non-inductive current drivers were investigated. Minority heating by ICRH appears to be one of the least efficient drivers, on a par with neutral beam injection. The most desirable current drive method appears to be pulsed injection of a relativistic electron beam, although pulsed techniques can also benefit other drivers.

A limiter/vacuum concept has been developed for impurity control and exhaust. The advantages of this concept are: (1) manageable heat loads on the collection medium; (2) high tritium burnup leading to low tritium inventory; and (3) engineering simplicity compatible with ease of assembly/disassembly and maintenance.

Although liquid lithium offers substantial advantages as a breeding material and coolant, the magnitude of the stored chemical energy is an important safety concern. The less reactive liquid metals and solid breeders were investigated. One of the difficult problems with solid breeders is the development of an efficient tritium recovery scheme to keep the tritium inventory in the blanket to a low level. Another difficulty with many solid breeders is a low tritium breeding potential. Trade-off studies comparing helium and water as coolants show clear

* Work supported by the US Department of Energy.

advantages for the use of pressurized water in tokamaks if the temperature of the structural material is limited to ~500°C.

The greatest uncertainties in the economics of future tokamak power plants are in the areas of plant availability and construction time. These are crucially dependent on ease of assembly, ease of maintenance, and component reliability.

1. INTRODUCTION

A team led by Argonne National Laboratory has carried out two major tokamak design studies: STARFIRE and DEMO [1,2]. The STARFIRE study completed in October 1980 focused on developing a commercial tokamak power plant. STARFIRE was considered to be the tenth plant in a series of commercial reactors. The key technical objective of the STARFIRE study was to develop an attractive embodiment of the tokamak as a commercial power reactor consistent with credible engineering solutions to design problems. The DEMO study, now in progress, is aimed at defining the goals and developing a conceptual design for a Demonstration Power Plant. The major parameters for STARFIRE and DEMO are given in Table I.

The DEMO under consideration is the device that will be constructed after the Fusion Engineering Device (FED). The DEMO does not need to be economically competititve. Rather it needs only to demonstrate that it can be extrapolated to an economically competitive device. The basic objectives of the DEMO are:

(1) Demonstration of a level of performance for all components in an integrated system, which performance is satisfactorily extrapolatable to a commercial reactor.

(2) Demonstration of component and system reliability, availability, and lifetime at a level that would be satisfactorily extrapolatable to a commercial reactor.

(3) Production and extraction of tritium in the blanket, with a net tritium breeding ratio greater than unity and an acceptably low tritium inventory.

The first objective defined above requires that all components would be operated at conditions (e.g. temperatures, stresses, radiation level, etc.) similar to those of a commercial reactor. This has to be achieved in a device with reasonably low capital cost. The size of a tokamak DEMO is limited to a narrow range. For given technological (e.g. maximum magnetic field) and physics (e.g. maximum beta) constraints, the minimum

TABLE I. MAJOR DESIGN PARAMETERS FOR DEMO AND STARFIRE

	STARFIRE	DEMO
Fusion power, MW	3500	920
Thermal power, MW	4000	1050
Net electrical power, MW	1200	290
Overall availability,%	75	50
Average neutron wall load, MW/m^2	3.6	1.8
Major radius, m	7.0	5.2
Plasma half-width, m	1.94	1.3
Plasma elongation (b/a)	1.6	1.6
Plasma current, MA	10.1	9.0
Average toroidal beta, %	6.7	8.0
Maximum Toroidal field, T	11.1	10.0
No. of TF coils	12	8
Plasma burn mode	continuous	continuous
Current drive method	rf (LH)	REB
Wall blanket structural material	PCA (SS)	PCA
Wall/blanket coolant	water	water
Tritium breeding medium	solid breeder	solid breeder or liquid metal

size is defined primarily by ignition requirements. The neutron wall load (P_{nw}) for this minimum size device is on the order of 1 MW/m^2 for the constraints imposed in the DEMO study. Based on the STARFIRE results, commercial tokamaks will operate at a P_{nw} ~ 3-4 MW/m^2. Therefore, it is desirable to operate the DEMO at P_{nw} much greater than 1 MW/m^2. The only viable method to achieve this is to significantly increase the size of the DEMO. Unfortunately, this would increase the thermal power and capital cost for the DEMO. We have selected the DEMO parameters so that P_{nw} ~ 1.8 MW/m^2, an intermediate value between those for FED and commercial reactors. Thus, the power density in the blanket will be a factor of 2 lower than that expected in a commercial reactor. This unfortunately large extrapolation factor is dictated by considerations of the capital cost for the DEMO. Table II shows the range of parameters considered for the DEMO as compared to those for the near-term and future commercial tokamak reactors.

TABLE II. RANGE OF PARAMETERS FOR DEMO

	TFTR	FED	INTOR	DEMO	STARFIRE
MWth	20 fusion	180/450	620	800-1000	4000
MWe (net)	--	--	>10	200-300	1240
R (m)	2.5	5.0	5.2	4.9-5.3	7.0
r_p (m)	0.9	1.3	1.2	1.2-1.3	1.9
Plasma elongation	1.0	1.6	1.6	1.6	1.6
B_{max} (T)	--	8/10	12	10	11
Wall loading (MW/m^2)	0.2	0.4/1.0	1.3	1.5-2.0	3.6
Availability	--	0.1-0.20	0.35	0.50	0.75
β	0.012	0.052	0.56	0.06-0.08	0.067
Q (plasma)	>1	5/50	60	>10	35
Plasma heating	neutral beam	rf	neutral beam rf backup	rf	rf
Impurity control	--	Pumped limiter	single-null divertor	pumped limiter	pumped limiter
Operating mode	pulsed 1.5-s burn	pulsed 100/50 (s)	pulsed 100-s burn	steady-state: driver?	rf-driver driver?
Lifetime	4×10^3 pulses	5×10^4 pulses	10^6 pulses	20 y	40 y
Tritium breeding ratio	--	experiment	0.6	>1.0	>1.0
Material first-wall blanket	SS (304 LN)	SS (316)	SS (316)	SS	SS (PCA)
Coolant	H_2O	H_2O	H_2O	H_2O	H_2O

No attempt is made in this paper to summarize all the results of the STARFIRE and DEMO studies. Instead, this paper is limited to discussing key issues in three areas: (1) steady-state plasma operation and evaluation of candidate current drivers; (2) pumped limiter and poloidal divertor options for plasma impurity control and exhaust; and (3) breeder blanket options. In addition, a perspective on key aspects of tokamak engineering and economics, as derived from these recent design studies, is given.

The organizations involved in these studies include Argonne National Laboratory, McDonnell Douglas Astronatics Company, General Atomic Company, Ralph M. Parsons Company, and Physics International Company.

2. STEADY-STATE/CURRENT DRIVER

Theory and experiments indicate the possibility that toroidal plasma currents may be maintained in tokamaks with noninductive external momentum sources to the electrons. This suggests that steady state may be an achievable mode of operation for tokamaks. Steady-state operation offers many technological and engineering benefits in commercial reactors. Among these are: (1) component and system reliability is increased; (2) material fatigue is eliminated as a serious concern; (3) higher neutron wall load is acceptable; (4) thermal energy storage is not required; (5) the need for an intermediate coolant loop is reduced or eliminated; (6) electrical energy storage is significantly reduced or eliminated; and (7) an ohmic heating solenoid is not needed, and external placement of the EF coils is simplified. It has been estimated that the combined benefits of steady state can result in a saving in the cost of energy as large as ~25-30%.

The penalty for steady-state operation comes primarily from potential problems associated with a noninductive current driver; in particular: (1) the electrical power requirements; (2) the capital cost; and (3) reliability and engineering complexity of the current driver. The magnitude of these problems varies from one current driver to another.

A large number of external drivers have been proposed which theoretically can sustain the toroidal tokamak current in a steady, noninductive state. Both plasma waves and particle beams have been suggested, and a survey of the most attractive candidates has been performed. We classify waves into three types for this discussion. High-phase-speed (HS) waves are those with toroidal phase velocities exceeding the electron thermal speed and which directly impart momentum to the circulating electrons. Examples of these waves, which have received

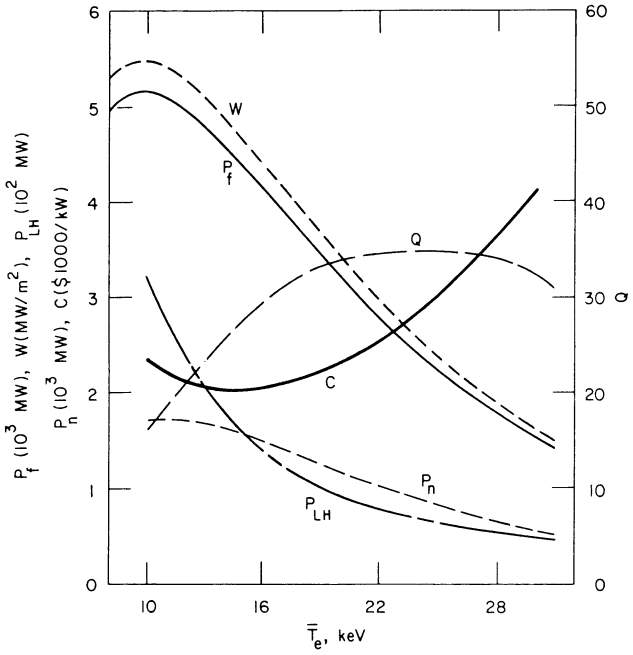

FIG. 1

Variation of fusion power (P_f) and lower hybrid wave power (P_{LH}) required to sustain the toroidal current with electron temperature for R = 7.0 m, B0 = 5.8 T, β_t = 0.067, and A = 3.6 (the STARFIRE reactor). Also shown are net electric power (P_n), reactor capital cost per unit power (C) including rf system, neutron wall load (W), and $Q \equiv P_f/P_{LH}$.

experimental tests for driving current, are the lower-hybrid wave (JFT-2 [3]), the magnetosonic wave (Synchromak [4]), and the ion-cyclotron wave (Model C [5]). Low-phase-speed (LS) waves are those with subthermal phase speeds which can supply electron momentum. The most studied example is the fast wave, which is the compressional Alfven wave at low frequencies and which we term a low-speed (short parallel wavelength) magnetosonic wave above the ion cyclotron frequency. The third wave-current-drive classification refers to ICRH and ECRH techniques which heat plasma to create anisotropic resistivity, thereby indirectly driving currents. Beam-driven currents may be created by injection of neutral beams (Culham Levitron [6]) or relativistic electron (REB) beams (SPAC-IV [7]).

Theory shows that all the drivers mentioned above become more efficient at lower electron densities (and, for a fixed beta, higher temperatures). One may write the ratio of absorbed power

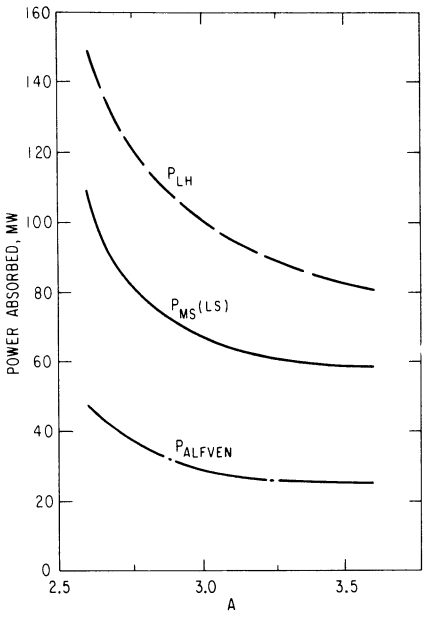

FIG.2

Power absorbed in plasma versus aspect ratio for P_f = 3400 MW, W = 3.6 MW/m^2, B_{max} = 11.1 T, and β_t = 0.25/A (the STARFIRE reactor). Drivers depicted are lower hybrid (LH), low- phase-speed magnetosonic (LSMS), and the compressional Alfven wave.

density to current density generated as $p/j \simeq 1.0 \times 1.0^{-18}(n_e/T_e)$ $\hat{p}/\hat{j}$, where density is in m^{-3} and T_e is in keV and $\hat{p}/\hat{j}$ is the normalized quantity discussed by Fisch [8]. In general, $\hat{p}/\hat{j}$ is determined by the dynamics of the current carriers and takes on different forms for different drivers [9]; $\hat{p}/\hat{j}$ is itself not a funct on of n_e. Thus, for a given equilibrium current density, j, the driver power is minimized by operation at the lowest densities. The tradeoff, of course, is that, for fixed beta, operation at low n_e requires high plasma temperatures, and, above ≃10 keV, the fusion power density decreases. Figure 1 shows this variation of fusion power (P_f) and driver power, in this case for lower-hybrid waves (P_{LH}). Although P_{LH} increases rapidly at low temperature, it is still very small compared to the fusion power so the net electric power (P_n) produced is still a maximum near 10 keV. However, the capital cost of the rf tubes and power supplies increases so quickly at low temperatures that the cost of power (C) increases for operation at temperatures less than ≃15 keV. Another study was done for reactors all having P_f = 3400 MW and a fixed neutron wall load W = 3.6 MW/m^2 with a maximum toroidal

field strength B = 11.1 T and inboard blanket/shield/scrapeoff Δ^i = 1.4 m, the STARFIRE values. However, the aspect ratio, A, was varied as well as the plasma beta -- $\beta = 0.25/A$. In going to smaller A both n_e and the toroidal curent, I, increase. Accordingly, the driver power must also increase at lower A. Figure 2 shows the variation of P_{LH} with A which motivated the selection of a large aspect ratio, A = 3.6, for STARFIRE. Lower-hybrid power requirements are so large that small A is not practical despite the fact that ohmic primary windings are absent from the central hole.

Lower-hybrid waves are a HS driver which forms a plateau on the tail of the electron distribution function. Theoretical values of $\hat{p}/j$ for HS waves are in the range 0.04 to 0.05 [8]. However, LS waves are more efficient with $\hat{p}/j$ values as low as 0.01. Figure 2 compares two LS drivers with the lower-hybrid wave. The main concern regarding the LS waves is that wave momentum is transferred to electrons with parallel velocities well below thermal; hence they are magnetically trapped. The implications of this neoclassical effect and its relationship to the bootstrap current are not well understood. Hence, the low power indicated in Fig. 2 for the LS waves is misleading, and the practicality of designing low A (high β) reactors is questionable since the power may be larger than shown in the figure. Our analysis of ICRH and ECRH is likewise disappointing. For the example of ^{3}He-minority-heating-induced current we find the best case has $\hat{p}/j \geq 0.07$, which is worse than the lower-hybrid driver.

From the engineering viewpoint, the lower-hybrid driver is attractive. The transmitter is an all-metal Brambilla waveguide array mounted flush with the first wall. Cross-field amplifiers are long lifetime, high efficiency tubes which should yield several hundred kilowatts at 1-2 GHz CW, and their power supplies do not need high regulation. Despite the high power reflection coefficient back into the array the overall electric-to-rf heating efficiency can be designed through the use of circulators and selected passive guides to approach 60%. Nevertheless, 150 MW of electric power is needed for the STARFIRE lower-hybrid driver, a large fraction of the gross electric power produced. In addition, wave accessibility constraints prevent wave propagation into the high-density plasma interior -- a hollow current equilibrium is formed. If higher β plasmas are a reactor design goal, then centrally peaked, high-current equilibria must be attained.

To this end we have identified the HS (long parallel wavelength) magnetosonic wave as a more desirable candidate in our optimization studies for the DEMO. The value of $\hat{p}/j$ is found to

be 0.03, which is lower than for lower-hybrid waves since transit time magnetic pumping appears to be more efficient than Landau damping according to Fokker-Planck studies [8]. In addition, this wave is not constrained by accessibility to low densities, so broad, centrally peaked currents are found in our ray-tracing calculations. Thus we feel that a high current, high beta ($\beta \approx 0.08$) discharge is a reasonable goal for the DEMO. Both reentrant (ridged-type) waveguides and short all-metal antenna loops appear to make reasonable transmitters, although the latter appear to allow the greatest control over wave frequency and spectrum. Water-cooled loops would be located 8-10 cm from the plasma edge and further protected by an all-metal Faraday screen. These loops are mounted on angle interfaces of the first wall where they average 10-15 cm separation from the return current in the wall, in order to provide good plasma coupling.

Neutral beam driver currents were calculated with a Monte Carlo particle code. Not unexpectedly, the results were no better than for the ICRH current drive method. Indeed, both minority heating and neutral injection create a circulating ion beam which transmits momentum to electrons. The most efficient technique for the DEMO would entail injection of 3-MeV neutral deuterium, which could only be achieved with rf accelerators [10]. The development of such a system, properly shielded for continuous operation, appears unjustified for a DEMO which would barely produce net electric power with this driver.

Pulsed injection of relativistic electron beams may, in fact, be the best means of driving toroidal current. In this scheme the REB is injected long enough (~10 μs) to establish a circulating runaway electron current which exceeds the initial plasma current. The reverse emf cancels most of the REB contribution, but a small increase, ΔI, in the total current occurs. After a period $\Delta t = (L/R)(\Delta I/I)$, determined by the plasma inductance and resistance, the pulse must be repeated. The increase ΔI depends crucially on the dc resistivity of the plasma return current [11]. If R remains neoclassical at all times then the time-averaged power required for the REB is identical with that for ECRH current drive in the relativistic limit, and the efficiency is no better than that of the lower-hybrid wave. However, REB injection appears to drive the two-stream instability which in turn may greatly increase the resistivity of the plasma return current. In this case, ΔI will be much larger, Δt will be increased, and, for a given REB energy in a pulse, $\mathscr{E}_b$, the average power, $P_{av} = \mathscr{E}_b/\Delta t$, will be decreased. If the resistivity exceeds neoclassical by a factor of $\sim 10^3$ the limiting case occurs; then the REB loses negligible energy via Coulomb collisions and instead transfers all its energy to the increased

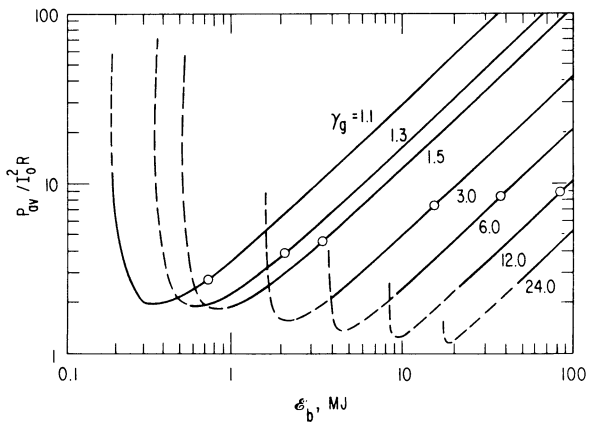

FIG.3
Time-averaged REB power normalized to equivalent ohmic heating power for pulsed REB current drive in STARFIRE, as a function of total beam energy per pulse. The relativistic mass to rest mass ratio is γ.

plasma current, viz $\mathcal{E}_b = \Delta\, {}^1\!/_2\,(LI^2) = LI\Delta I$. At this point the energy $\mathcal{E}_b$ is stored inductively in the poloidal fields, and hereafter a forward emf drives the current "ohmically". So, in this limit the average power approaches the ohmic heating value: $P_{av} = \mathcal{E}_b/t\Delta = \mathcal{E}_b/[(L/R)\Delta I/I] = \mathcal{E}_b RI/[L(\mathcal{E}_b/LI)] = I^2R$. Figure 3 displays the results of a more detailed calculation [11] for STARFIRE, assuming the resistivity is enhanced by a factor $\gtrsim 10^3$ during the REB lifetime. If the return current's resistivity is not enhanced by such a large factor (e.g., if the two-stream instability is not excited) the reverse emf will be weaker and more of the REB momentum is wastefully dissipated against the plasma ions. In such a case Fig. 3 would underestimate the average power requirement.

The DEMO design calls for a relativistic $\gamma = 4$ (1.5 MeV) beam delivering 4 MJ to the plasma about every 1.5 s. The coaxial transmission line has several bends and passes through a 50-cm diameter port in the blanket. A plasma diode [7] is specified which appears compatible with the reactor environment. The Marx banks, tubes, and switches can be in a separate building.

The success of REB current drive relies heavily on the wave-enhanced resistivity of the return current. It may be possible to extend these benefits of pulsed power injection to other drivers, including waves. In this case, the resistivity could perhaps be increased temporarily in a controlled fashion, e.g. by increasing Z_{eff} of the plasma. This may present a more

reliable means of oscillating plasma resistivity, although the reduction in time-averaged power compared to the continuous current drive power may be less dramatic than for the REB.

3. IMPURITY CONTROL

The impurity control and exhaust system poses some of the most difficult problems in tokamaks. Therefore, the STARFIRE and DEMO studies have devoted significant effort to the development of a credible and attractive design for this system. Two concepts were considered: a pumped limiter and a poloidal divertor.

3.1 Limiters

Besides providing for adequate impurity exhaust, a limiter impurity control system must serve several other functions. The limiter system should:

(1) Be capable of operating under high heat flux conditions.

(2) Withstand the electromatic effects of periodic plasma disruptions.

(3) Have an adequate lifetime ($\geq$1 y at maximum duty factor).

(4) Be replaceable independently of the first wall and blanket components.

(5) Have a minimum impact on the tritium breeding.

A limiter/vacuum impurity control system that appears to meet these requirements was developed for both the STARFIRE and DEMO designs. The limiter design for STARFIRE is shown in Fig. 4 and key design parameters for both systems are listed in Table III. Both designs use a toroidal belt limiter located on the outboard side of the torus. Some differences in design parameters are due to the different size and power levels of the two reactors and others are due to intentionally using different plasma physics parameters in order to explore a range of design possibilities. Both limiters consist of a front face, two "leading edges", and a slot region formed between the leading edges and the first wall. A vacuum duct system, consisting of various paths through the torus is connected to the limiter at one end, and to a series of cryopumps at the other. The entire surface of the limiter, as well as the first wall, is coated

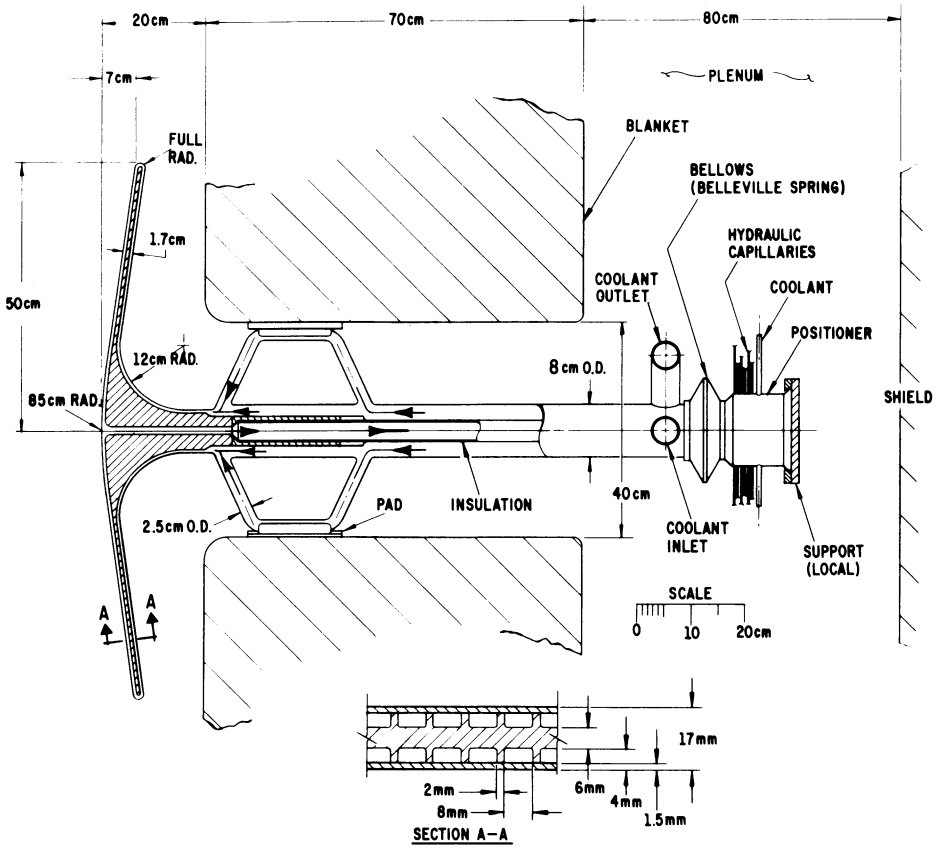

FIG. 4
Cross section of the STARFIRE limiter design.

with a low-Z coating to avoid sputtering of the highly radiative structural material. Beryllium was chosen as the low-Z coating material but other materials, notably C, SiC, B, and B_4C are also candidates.

The limiter operates as follows. Ions from the plasma (D, T, He, and Be) that strike the front face of the limiter and the leading edges are neutralized and recycled back to the plasma. Ions entering the slot region are neutralized at the bottom of the slot where most tend to be trapped, and these are eventually removed by the vacuum system. It is fairly well established that trapping and the subsequent high neutral pressure and high pumping probabilty of particles entering the slot region occur

because of (1) ionization of neutrals by the incoming plasma; (2) momentum transfer from the plasma to the ionized neutrals; (3) pre-sheath electric field effects; and (4) ballistic scattering of the incoming ions on the neutralizer surface. Because of these effects the conductance (for molecular flow) of the vacuum system need only be a small fraction (typically F0.20) of the limiter slot conductance for adequate pumping. This is the case for both STARFIRE and DEMO designs and will probably be so for most reactor designs.

The limiter/vacuum system, as with other impurity control systems, must remove helium atoms from the plasma at the rate

TABLE III. LIMITER/VACUUM SYSTEM RELATED PARAMETERS FOR STARFIRE AND DEMO

	STARFIRE	DEMO
Type of limiter	Toroidal belt type on midplane	Same
Reference structural material	TA-5W, AMAX-MZC, FS-85, V-20Ti, or Cu & Cu alloys	Same
Low-Z coating	Be	Be
Type of vacuum pumps	Cryopumps	Cryopumps
Transport power to limiter, MW	90	~90
Plasma edge temperature, keV	1.2	1.5
Energy e-folding distance in scrape-off zone, cm	5.0	2.7
Location of leading edge, cm	7.0	7.5
Heat load on leading edge, MW/m^1	3.6	2.3
D-T current at plasma edge, s^{-1}	3.5×10^{22}	6.4×10^{22}
He production rate, s^{-1}	1.2×10^{21}	6.4×10^{20}
He pumping efficiency, %	25	10
He concentration in plasma, %	14	5

they are produced by fusion. There is, however, a wide combination of plasma helium densities and helium removal efficiencies that satisfy this condition. For example, a tokamak could be operated at high helium plasma concentration and low removal efficiency, or the converse. The tradeoffs between these are as follows: a high helium removal efficiency minimizes the helium concentration in the plasma but increases the hydrogen gas load, increases the tritium inventory, and makes for a more difficult limiter design. A low helium removal efficiency minimizes the hydrogen gas load and the tritium inventory, eases the limiter design, but incrases the plasma helium concentration. Plasma transport code studies, e.g. Ref. 12, have also shown that the particle flux at the plasma edge may itself depend on the pumping efficiency, and this introduces another factor to the tradeoff situation. The STARFIRE design uses a moderate pumping efficiency of 25% which, together with the reference particle outflux, results in a high helium concentration of 14% in the plasma. This is compensated for by designing the toroidal field coils to have an extra "field margin" of about 1.0 T. Thus, some of the burden of the impurity control system is shifted to the TF system. The DEMO design employs a different operating regime whereby only 10% helium removal is used but at a higher particle outflux. The resulting helium concentration is on the order of 5%. It is uncertain at this time whether a limiter or divertor will have any helium enrichment properties, whereby plasma-neutral interactions in the slot region will preferentially release hydrogen back to the plasma but trap helium. Helium enrichment is not a vital consideration but would serve to further minimize the tritium inventory in the vacuum and tritium handling systems.

The heat load to the limiter is a key engineering issue. The limiter heat load is primarily due to thermal transport from the plasma with additional heating due to X-rays and neutrons. Both STARFIRE and DEMO designs reduce the transport heat load by operating the plasma in an "enchanced radiation mode", whereby a high-Z material, nominally iodine, is intentionally added to the plasma to radiate as much heat as possible to the first wall. This mode of operation appears to be possible for any large tokamak ($R \gtrsim 5$ m) because of the large margin for ignition, at least if empirical electron and neoclassical ion energy confinement scaling is assumed. The fraction of alpha power radiated varies from ~50% in DEMO to ~80% in the larger STARFIRE device. For a fixed value of transport power, the heat flux to the limiter is minimized by (1) angling the front face so as to spread the heat over a wide area; and (2) locating the leading edges ~1-2 energy e-folding distances into the scrapeoff zone. The limiter front face can also be shaped to keep the heat flux nearly constant over most of the surface, and this strategy was

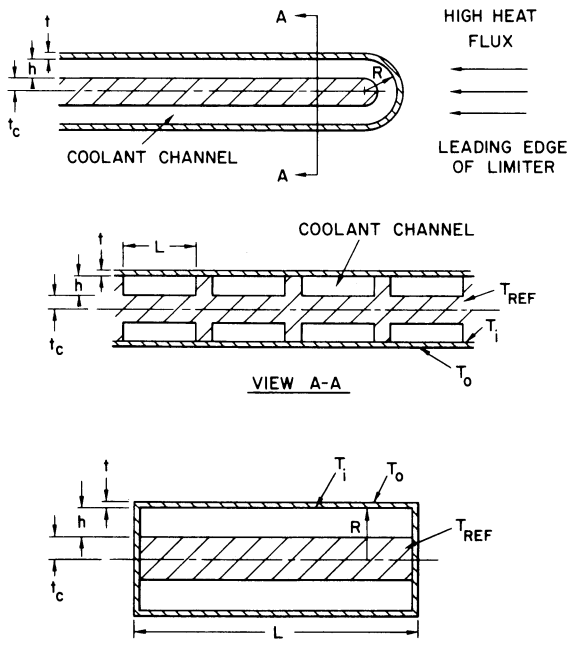

FIG.5
Cylindrical model of a typical coolant channel at leading edge.

adopted for the DEMO design. For future large power reactors where e-folding distances and other plasma parameters will presumably be known in advance the outboard belt limiter functions well. For a nearer-term experimental device, the "bottom limiter" [13] concept may be a better choice as it is less sensitive to changes in scrape-off parameters from the design values. The limiter heat load for DEMO and STARFIRE, and probably for most other devices as well, is in the range of 2-4 MW/m^2. The structural materials with the greatest capability of operating at these and higher heat loads (up to ~10 MW/m^2) are the refractory metal alloys, such as the vanadium, niobium, tantalum, or tungsten alloys, and copper and copper alloys. Stainless steel, both austenitic and ferritic, cannot be used because of its relatively poor thermophysical properties. The most attractice coolants for the limiter are water and liquid metals. Water coolant was chosen for STARFIRE. Helium coolant can be eliminated from consideration due to its poor heat transfer characteristics. The refractory metals are not compatible with high temperature water and therefore their use at high temperatures would likely be restricted to liquid metal coolants. Copper alloys are generally thought to be compatible with high temperature water but not with liquid metals. The heat load on the

TABLE IV. STRESSES (MPa) AT LEADING EDGE OF LIMITER

Material	$\sigma_s^{P(a)}$	$\sigma_x^{P(b)}$	$\sigma_x^{G(b)}$	$\sigma_x^{G(b)}$	$\sigma_s^{T(c)}$	$\sigma_x^{T(c)}$	$\sigma_s^{(d)}$	$\sigma_x^{(d)}$	σ	Ratio of σ to Yield Stress
Tantalum, Ta-5W	-12	-38	-103	-82	-185	-242	-197	-280	249	0.73
Niobium, FS-85	-12	-38	-195	-156	-305	-370	-317	-408	371	1.00
Vanadium, V-20Ti	-12	-38	-300	-240	-458	-576	-470	-585	537	1.19
Copper, AMAX-MZC	-12	-38	-28	-22	-102	-167	-114	-205	178	0.41

[a]Contribution due to pressure.

[b]Contribution due to temperature gradient.

[c]Total contribution due to temperature.

[d]Final values of stress components.

limiter could either be recovered as sensible heat and used for electricity production, as with STARFIRE, or simply dumped as waste heat, as with the less demanding DEMO design.

The response of candidate limiter materials to high heat flux conditions was examined for the STARFIRE design. Specifically, the sresses at the leading edge of the limiter, which receives a heat flux of ~4 MW/m^2, have been calculated and compared with design allowable stresses. The leading edge consists of a 180-deg cylindrical shell as shown in Fig. 5. The coolant channel rib structure is welded to the outer cylindrical shell. For the stress calculations, the radius of the cylinder was assumed to be 8.5 mm, the coolant channel width was 8.0 mm, and the wall thickness of the cylindrical shell was 1.5 mm. The stresses at the leading edge are due to the internal coolant pressure, the temperature gradient through the outer wall, and the temperature difference between the coolant rib and the cylindrical shell. Table IV shows the results of the stress calculations for four alloys. The subscripts s and x in the table refer to the circumferential and axial directions respectively. The effective stress, σ, is defined by:

$$\sigma = \left(\sigma_x^2 + \sigma_s^2 - \sigma_x\sigma_s + 3\tau^2\right)^{1/2}$$

where τ is shear stress (zero for this design). In general, the thermal stresses dominate the combined effective stress. The copper alloy AMAX-MZC, has the lowest calculated stress, both in absolute and relative terms, due primarily to its high thermal conductivity. The tantalum alloy, Ta-5W, has the next lowest stress, and is also an acceptable material for this design. The other refractory metal alloys exhibit significantly higher stresses, but they are probably acceptable materials for lower heat flux designs.

The most critical issue for a limiter impurity control systems is probably sputtering and erosion of the surface. Because the low-Z materials do not have adequate structural strength to be used alone, a duplex structure is used for the first wall and limiter, whereby the low-Z coating or cladding is supported by the structural metal alloy. A major concern in the design of duplex structures is the large stresses that could occur accross the materials interface due to the large differences in properties. At very low plasma-edge temperatures, low-Z materials may not be required since the D-T sputtering of moderate Z materials would be low, and the self-sputtering coefficient is likely to be <1. The elimination of the low-Z materials would simplify the engineering design, but there is a large uncertainty at this time whether low-edge temperatures can be attained.

Sputtering of the low-Z coating/cladding depends on the coating material, plasma-edge temperatures, and the particle flux. For both STARFIRE and DEMO, transport code studies predict an edge temperature greater than 1 keV at the start of the scrapeoff zone. Together with the sheath potential, ions would strike the limiter with multi-keV energies over the whole surface. This actually helps minimize sputtering of the low-Z coatings since sputtering yields tend to peak at lower energies. For example, D-T sputtering of beryllium peaks at ~400 eV and decreases at higher energies at approximately a linear rate. The most important issue associated with sputtering, however, is probably the redeposition of sputtered material on the limiter and the transfer of sputtered material from the first wall to the limiter. Redeposition of sputtered material occurs as follows: sputtered impurity atoms emerge from the limiter surface at random angles (typically a cosine distribution) and at energies of few eV. Many of these atoms do not travel far (a few cm) before they are ionized by electron-impact collisions in the scrapeoff region. Once ionized the impurity ions stick to a field line where momentum transfer with the incoming plasma brings them back to the limiter surface. Since the self-sputtering coefficient of the low-Z materials is much less than unity, most of the returned ions "stick" or redeposit on the surface. The only impurity atoms that do not immediately redeposit are those that flow out of the scrape-off zone before being ionized. However, even these eventually come back to the limiter (along with the D-T or helium outflux) and tend to stick. There is also a transfer of wall coating material, sputtered by charge-exchange neutrals, to the limiter. (Because of the geometry of the STARFIRE and similar limiters, transfer of material from its limiter to the wall is unlikely). An analysis [14] using a code that models these effects indicates that the redeposition and wall-to-limiter transfer is so substantial that the limiter coating, instead of eroding, could actually grow with time. As a result, excess coating might have to be removed periodically, e.g. by a grinding process. However, this may be much easier than recoating.

Results from a typical calculation using this code are shown in Fig. 6 for the DEMO limiter. This calculation used a somewhat simplified geometry whereby the limiter is represented by two straight lines, one of 7.5-cm (in plasma radial dimension) representing the front face and one of 1.0 cm representing the leading edge. The first wall is located 8 cm from the end of the leading edge. In addition to the effects mentioned, the code models the D-T density and temperature in the scrape-off zone, sheath potentials at the limiter, and sputtering coefficients for D-T and self-sputtering at the limiter, and D-T charge-exchange sputtering at the first wall. Plasma parameters

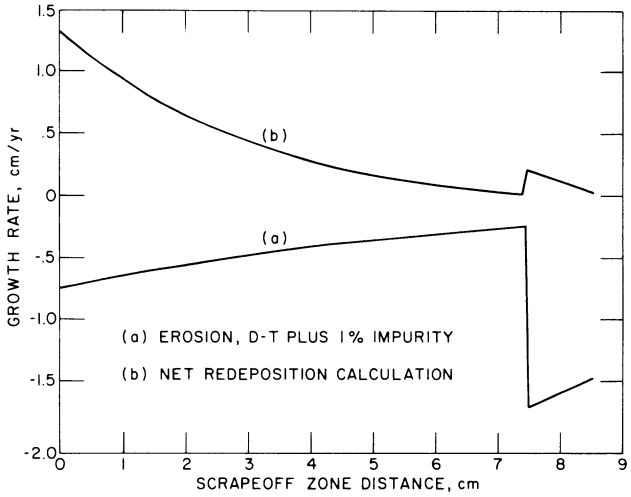

FIG.6
Growth rate on the limiter with and without redeposition.

corresponding to one-dimensional transport runs for DEMO with rf-current drive were used. A plasma beryllium concentration of 1% was used; most of this comes from wall and limiter sputtering with an additional amount added to the plasma from an external source. Curve (a) shows the growth rate along the surface of the limiter if no redeposition whatever is assumed. The growth rate is negative meaning that only erosion occurs. Erosion averages about 0.5 cm/y on the front face to about 1.5 cm/y on the leading edge. (This calculation is for 100% duty factor. DEMO would use much less.) When redeposition is included, curve (b), the limiter coating grows everywhere. The growth rate varies from near zero at the leading edge to ~1.5 cm/y at the limiter tip. Other runs have shown that a fair control over growth rate may be achievable by varying parameters such as the limiter geometry, edge temperatures, and plasma impurity content. These calculations are, of course, dependent on uncertain plasma physics calculations and uncertain materials properties. Questions about the integrity of the redeposited surface as well as the entire area of redeposition physics must be confirmed by experiments; however, this process offers substantial hope for extending the limiter lifetime.

Several other factors besides sputtering can influence the lifetime of the limiter system. These include thermal fatigue failure, radiation damage, and corrosion and stress cracking. Thermal fatigue can be reduced by the proper selection of material and by reducing the number of operating cycles. It is

desirable, therefore, to have a long burn time, and steady-state operation, as assumed for both STARFIRE and DEMO, should practically eliminate the thermal fatigue problem. Radiation effects are a key concern for the structural material. As a class, the refractory metal alloys appear to be more resistant to radiation damage than copper or copper alloys. The available radiation data is sparse in many areas, however, and further experimental effort is needed. Corrosion and stress-corrosion cracking should be controllable by the proper coolant selection, but continuous control of the coolant chemistry will be required.

Plasma disruptions can affect the limiter lifetime in two ways. If the limiter receives most of the plasma energy during a disruption, then a portion of the surface will be lost due to vaporization and/or melting. In addition, large thermal stresses will be generated, which could affect the materials microstructure and lifetime. The effects of a disruption can be minimized by reducing the total number of disruptions or by placing the limiter in a position where disruptions are least likely to strike. At present, it is believed that the disruption energy is most likely to strike the inboard, top, and bottom sections of the torus. The most desirable location for the limiter is therefore at the outboard midplane. The second effect of disruptions is the magnetic torque which is caused by the interaction of the current induced in the limiter during a disruption and the toroidal magnetic field. This effect can be minimized by using metals with low electrical conductivity, reducing the length of the current path, and providing sufficient structural support for the limiter.

3.2 Poloidal Divertor

Impurity control with a divertor is accomplished by magnetically diverting ionized particles, located at the edge of the plasma, out of the plasma chamber and ultimately into the vacuum pump system. The particles at the plasma edge include both the D, T, and helium ions escaping from the plasma and the sputtered atoms from the first wall. A divertor system requires additional magnets to reshape the magnetic field for the divertor effect plus an additional vacuum chamber(s) that serves to neutralize the ionized particles and to convert the incoming particle energy into heat which is conducted out of the chamber by the coolant. The energy conversion and particle neutralization occurs when the particles strike the divertor collector plates in the divertor chamber. Because of the high energy and high flux of the incoming particles the collector plates will be subjected to severe operating conditions. The potentially high surface heat flux and sputtering make the operating characteristics of the collector plate analogous to those of the limiter.

The general requirements for divertor systems are the same as those discussed previously for limiter systems. However, there are several important differences from limiters that affect the design flexibility of divertors. First, calculations from the INTOR design studies predict that the sputtered first wall particles will all be directed to the divertor and will not enter the plasma [15]. Therefore, it is not necessary to have a low-Z material facing the plasma, which expands the available materials choices and should simplify the first-wall design. Second, the collector plates are outside of the plasma chamber reducing the backstreaming of impurities to the point where the use of low-Z materials is not necessary. In addition, the large volume associated with the divertor chamber provides greater flexibility in the design of the impurity control components. In particular, the collector plates can be placed at glancing angles with respect to the incoming particles, thus reducing the maximum heat and particle flux. The collector plates do not have a leading edge like most limiter concepts which also reduces the problems associated with high heat fluxes and thermal stresses.

The problems associated with divertors stem from the large volume associated with the divertor chamber(s), the additional magnets required, and the potentially short lifetimes of the divertor collector plates. The divertor chamber must be accommodated within the toroidal field coils and will affect the accessibility and maintainability of other reactor components. The magnets required for the divertor will also affect the accessibility and will, as well, increase the cost of the magnet systems.

The potentially short lifetimes of the collector plates have several implications. The high sputtering rate is due, in part, to high recycling rates of deuterium and tritium between the plate and the incoming plasma, within the divertor channel. The high sputtering rate of the collector plate is likely to determine the lifetime. Maximum lifetime can be obtained by selecting the material with the lowest sputtering coefficient. For a typical plasma energy of several hundred eV, tungsten is expected to have the lowest sputtering rate, but it is a poor structural material in the irradiated condition and it is difficult to fabricate. In order to insure adequate structural integrity, a standard structural material is required to support the tungsten and to carry the coolant. This combination results in a duplex structure with the potential for high stresses at the materials interface, due to the differences in the materials properties. The use of a low sputtering material is still likely to result in rather short lifetimes, and provision must be made to replace the collector plates at regular

intervals (approximately every two years). The replacement time and requirements can be minimized by designing a separate divertor module that is nonbreeding. A nonbreeding module would significantly reduce the tritium breeding capability, and thus restrict the possible choice for breeding materials.

The above considerations have been used in designing the divertor system for the DEMO. This design is similar in many respects to that of INTOR [15,16]. A single-null poloidal divertor located at the bottom of the plasma chamber was selected to minimize the engineering complexity and volume of the divertor system. Additional poloidal field coils are provided to reshape the magnetic field. The entire divertor chamber is designed to be easily removed at regular intervals so that the sputtered collector plates can be replaced. For INTOR, the divertor chamber is nonbreeding, and the breeding ratio is estimated to be only ~0.6 using Li_2SiO_3 material. For the DEMO where a breeding ratio of >1 is required, the region surrounding the divertor chamber would have to breed tritium if solid breeders are used. A liquid-metal breeding option is also being considered, in which case a breeding ratio of >1 can be obtained without tritium breeding in the divertor chamber.

The problems associated with the collector plate design have been addressed in INTOR [15,16]. A total heat flux of 70 MW and a total particle flux of 5.5×10^{23}/s is directly incident on the inner and outer collector plates. The plates are placed at glancing angles with respect to the separatrix which results in a maximum heat flux of 2 MW/m^2 and a peak particle flux of 1.5×10^{22}/m^2-s. The incident particle energy is assumed to be 400 eV. The overall collector plate design, shown in Fig. 7 , consists of a tungsten protection plate that is mechanically attached to the heat sink composed of Type 316 stainless steel. It is estimated that the protection plates must be replaced at approximately 2-y intervals, when the reactor is operating at a 50% duty factor, due to material loss by physical sputtering. The mechanical attachments result in poor thermal conductance between the protection plate and heat sink, but allow the protection plate to freely expand and rotate during the burn cycle, thus minimizing the thermal stress. During the burn cycle, the plate temperatures increase to 2000-2400 C, at which point 40 to 50% of the incident heat is radiated back to the divertor and plasma chambers, reducing the thermal gradient in the protection plate and the heat flux incident on the heat sink. The reduced heat flux on the heat sink of ~1.1 MW/m^2 makes it possible to use Type 316 stainless steel, which can tolerate only low heat fluxes due to its poor thermophysical properties. Type 316 stainless steel does, however, have adequate radiation damage resistance and mechanical properties to

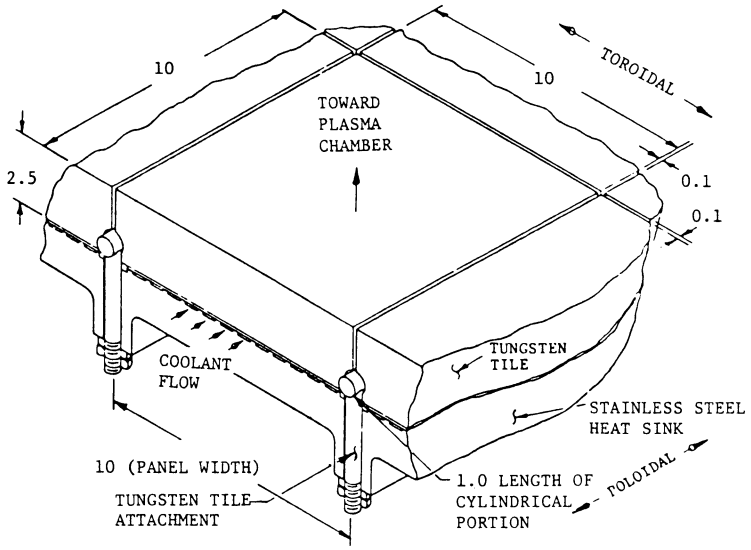

(a) Isometric cutaway through typical plate assembly.

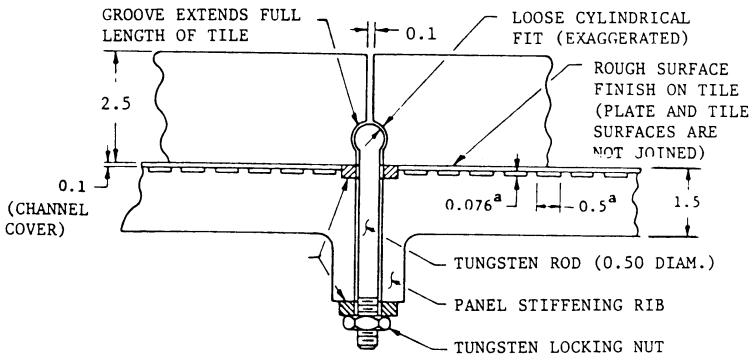

[a]Channel dimensions shown are for peak heat flux region only.

[b]All dimensions in cm.

[c]All dimensions are typical.

(b) Cross section through typical plate assembly (full scale; looking in poloidal direction).

FIG.7

Reference divertor collector plate design.

last the lifetime of the reactor. The major concerns with this design are the potentially high chemical sputtering rates of the tungsten, if the oxygen impurity in the incoming particle flux is $\gtrsim 0.5\%$, and the potentially low emissivity values of the tungsten surface that could result in unacceptably high operating temperatures.

There are several key areas where additional information is required to more adequately assess divertor designs. First, the plasma physics in the area just above the collector plates is not well understood. In particular, most of the particles sputtered from the collector plates may be redeposited, but the physical processes involved are not clearly understood. Second, additional physical sputtering experiments are needed, since the sputtering coefficients are usually known only to within a factor of two. For several materials, like carbon, tungsten, and molybdenum, chemical sputtering could be significant. Both the impurity level and the chemical sputtering coefficients should be known more accurately. Third, there is a need for mechanical property data for several materials. The general requirements for divertor materials often lead to the selection of specialized materials for which there are few mechanical property data. Information of particular interest includes fatigue data of high-Z refractory metals, radiation effects data for copper and copper alloys, and bonding characteristics of braze materials in a radiation environment.

4. SOLID BREEDER BLANKET

The objectives of the present study involve identification of key technological constraints of candidate tritium-breeder blanket concepts, establishment of a basis for assessment and comparison of the critical problem areas and design features of each concept, and development of optimized blanket designs. The focus of current work is on more detailed analysis of solid breeder blanket designs. Because of the attractive neutronic properties emphasis in the DEMO study is placed on the potential of Li_2O as a breeding material. The $LiAlO_2$ proposed in the STARFIRE study is considered the reference ternary ceramic, which is characteristic of other possible compounds such as Li_2ZrO_3 and Li_2SiO_3.

General features of the STAFIRE blanket design that are retained in the DEMO include containment of high pressure coolant in small tubes dispersed throughout the breeder region and the use of a low-pressure helium purge for in-situ tritium recovery. Recent work summarized here has been devoted to both the materials data base and generic design issues. Specific materials-related work includes fabrication of ceramics, thermal

conductivity measurements, tritium solubility measurements, analysis of chemical stability, compatibility with candidate structural materials, and gas phase migration (percolation) of tritium through porous breeder materials. Design issues relate to tritium breeding, thermal-hydraulics, and coolant selection. References 1 and 17 have more details.

4.1 Materials Data Base

4.1.1 Fabrication

Fabrication of high purity Li_2O, $LiAlO_2$, Li_2ZrO_3, and Li_4SiO_4 has been accomplished [18,19]. Several problems encountered in the preparation of high purity Li_2O provide considerable insight into compatiblity and stability problems that will be encountered in a Li_2O breeder blanket. Preparation of Li_2O by thermal decompositon of Li_2CO_3 under vacuum (~10^{-3} Pa) at 1153 K (880°C) led to significant contamination of the Li_2O by Pt, Ni, Ta, and Zr crucible materials. Typical analyses revealed >1000 wppm of the container materials in the oxide after exposure for only ~20 h during the decomposition. Much less contamination (~10 wppm) occurred when the Li_2CO_3 was rapidly heated (~4 min)to 1223 K for the decomposition of Li_2CO_3. With good vacuum pumping to remove the CO_2, decomposition was completed in ~0.5 h.

Attempts to sinter the Li_2O also revealed important information regarding the use of Li_2O at high temperature. Minor but measureable amounts of Li_2O volatalizied during sintering for 4-6 h at 1323 K in a pure oxygen environment. In contrast, with a reducing atmosphere, as much as 90% of the pellet mass was lost in 4-6 h during sintering at 1323 K. The high oxygen partial pressure greatly reduces the decomposition rate of Li_2O. These results indicate that the maximum temperature of a Li_2O blanket must be kept significantly below 1300 K since the purge stream is not highly oxidizing and the exposure time will be very long.

4.1.2 Thermal Conducitivity

Measurements of the thermal conductivities of candidate ceramic breeder materials have recently been made [20]. Figure 8 summarizes the recent results for $LiAlO_2$, Li_2ZrO_3, and Li_4Si_4. Results obtained for 84% TD $LiAlO_2$ at temperature below 773 K are slightly higher than previous data reported by Gurwell for 89% TD material. High-temperature results (1173 K) for 78% TD material gave conductivity values of ~2 W/mK [21], which is in good agreement with extrapolation of the other data. Data for 89% TD Li_4SiO_4 are slightly lower than the values for

THERMAL CONDUCTIVITY OF LITHIUM CERAMICS

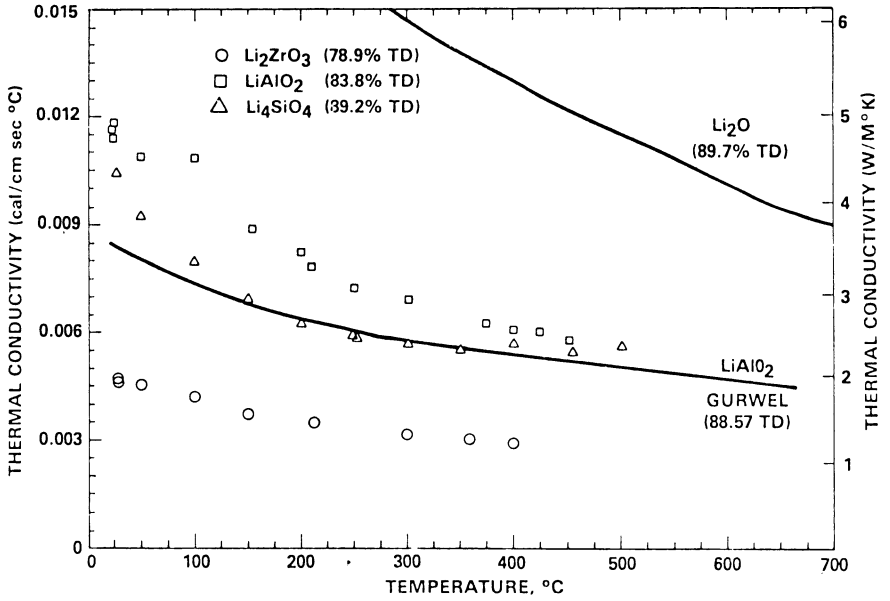

FIG.8
Thermal conductivity of $LiAlO_2$, Li_4SiO_4, Li_2ZrO_3, and Li_2O.

$LiAlO_2$. Results for Li_2ZrO_3 (79% TD) are about half the values for $LiAlO_2$. The thermal conductivities of all three binary compounds are considerably less than the values for 90% TD Li_2O reported by the Japanese [22].

4.1.3 Tritium Solubility

By means of gas-solid equilibration techniques, the apparent solubility of LiOH in Li_2O has been estimated to be 30 wppm at 1098 K [17]. This corresponds to an estimated hydrogen concentration of 1 wppm. The results were based on quantitative measurements of moisture evolved from Li_2O when the sample temperature was reduced to 1098 K after equlibration in helium containing 65 vppm H_2O. The process was reversed upon heating to 1123 K. These results are in fair agreement with values of 0.4 ppm tritium in Li_2O at 923 reported by Nasu, et al [23].

4.1.4 Chemical Stability

The potential for considerble mass transfer of lithium from a Li_2O blanket, probably in the form of LiOT in the purge

stream, was discussed in the STARFIRE report [1]. Limited experimental data presented [24] indicated that significant weight loss occurred when Li_2O was exposed to helium containing small amounts of H_2O. Calculations [18] based on experimental data indicate equilibrium LiOH partial pressures of 7.5×10^{-3} and 2.0×10^{-3} Pa over Li_2O at 1123 K for carrier gas moisture concentrations of 60 and 3.4 vppm H_2O, respectively, For the STARFIRE conditions a T_2O pressure of 0.1-1 Pa in the purge stream was required for reasonable purge stream flow rates of 10 and 1 m^3/s, respectively. For a helium pressure of 0.05 MPa, a T_2O pressure of 0.5 Pa corresponds to 10 vppm. From the above data, the equilibrium LiOH pressure under these conditions would be 6×10^{-3} Pa at 1123 K. These values correspond to possible losses of the order of 6 kg/y of LiOT from a Li_2O blanket. Analyses conducted concluded that maximum Li_2O temperatures might be limited to less than 650°C to avoid excessive lithium mass transfer in the purge stream.

4.1.5 Compatiblity with Structure

The compatiblity of solid breeder materials with candidate structural materials is an important consideration in the development of a solid breeder blanket. Chemical reactions between structure and breeder could impact the mechanical integrity of the structural material and the tritium release characteristics of the breeder. Compatibility tests have been conducted at temperatures of 873 and 973 K with Li_2O, $LiAlO_2$, and Li_2SiO_3 [25, 26] and at 823 and 923 K with Li_2O, Li_2ZrO_3, and Li_2TiO_3 [27]. In all cases Li_2O is the most corrosive of the breeder materials tested. Reaction phases observed after exposure of Li_2O, $LiAlO_2$, and Li_2SiO_3 to the stainless steel, HT-9 alloy and Inconel 625 included $LiCrO_2$, $LiFeO_2$, Li_5FeO_4, and $Li_2Ni_8O_{10}$. Total scale thickness for Type 316 stainless steel exposed to Li_2O at 873 and 973 K for ~2000 h was ~50 μm [24]. Further work is required to evaluate the time dependence of the interaction. Estimates based on parabolic rate constants for several hundred-hour tests are quite large for the proposed blanket lifetimes [27].

4.1.6 Percolation Model

The method of tritium recovery proposed in the STARFIRE design included migration of T_2O from the surface of the Li_2O grain through interconnected porosity to the helium purge stream. In the STARFIRE design a bimodal pore distribution in the ceramic breeder was used to facilitate this transport mechanism. Calculations based on two-phase gas flow, i.e., T_2O in helium, indicate that the bimodal pore distribution provides significantly better tritium release rates than a monolithic

structure with the same effective density of 60-70% TD. For the relative grain-to-particle size distribution suggested for the STARFIRE design, viz, 1 μm grain and 1 mm particle, gas migration within the particle appears to be the more critical rate limiting process. Further analyses to determine the optimum ratio of grain size to particle size are in progress.

4.2 Tritium Breeding Potential

Fusion reactors are required to produce more tritium than they consume. The excess tritium is used to supply the initial inventory for new reactors. The required tritium breeding ratio (T) is a function of many parameters, the most important of which are the desired doubling time and the equilibrium tritium inventory in the blanket. For a doubling time of $\geq$10 y and a blanket tritium inventory of $\leq$10 kg, the required T can be as low as 1.01. However, the designer must allow for some margin to compensate for uncertainties in nuclear data and calculational methods. Sensitivity analyses indicate that such uncertainties may be on the order of 10%. There are also uncertainties associated with the definition of the design details of the reactor system; e.g. size and shape of penetrations, structural material, coolant requirements, etc. Therefore, the designer must strive to develop a blanket design that yields a T $\geq$ 1.1. This is the net tritium breeding ratio in a realistic design with all engineereing details, such as penetrations and heterogeneity accounted for.

A significant effort was devoted in the STARFIRE and DEMO studies to estimate the breeding potential of all promising breeder materials in blanket designs that satisfy all known engineering constraints. Furthermore, calculations were made in realistic tokamak-reactor geometries. The results show that the most promising breeding materials can be classified according to their breeding potential into three categories. Category A includes liquid lithium and lithium-lead and lithium-lead-bismuth alloys. Breeder materials in this category can be utilized in realistic blanket engineering designs to yield a net tritium breeding ratio as high as 1.3. Thus, there is sufficient margin here to compensate for data and calculation uncertainties. Furthermore, a good portion of the space-limited inboard region of a tokamak does not need to be occupied by breeding materials.

Catergory B includes Li_2O. The best blanket designs in STARFIRE- and DEMO-type reactors yield a net tritium breeding ratio that is limited to ~1.1-1.15. Thus Li_2O seems to provide adequate margin to compensate for data and calculation uncertainties. However, the margin does not appear to be large enough to eliminate the inboard breeding blanket. The benefits

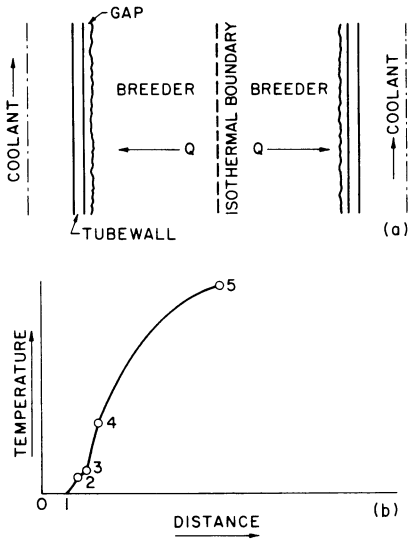

FIG.9
Schematic of a blanket segment and temperature distribution in breeding region (not to scale).

obtainable by the use of neutron multipliers with Li_2O are small.

Category C includes the ternary lithium oxides such as Li_2SiO_3, and $LiAlO_2$. An effective neutron multiplier is necessary with these materials to obtain $T > 1$. Optimization studies show that the net tritium breeding ratio obtainable with the ternary ceramics is limited to ~1.05-1.1. This low breeding potential is a serious cause for concern. Although the achievable breeding ratio is above the required minimum of 1.01, it does not include enough margin to compensate for uncertainties in data, calculation, and design. Although these breeding ratio estimates do not rule out the ternary ceramics, integral breeder experiments are necessary to provide a better assessment of the breeding potential for these breeder materials.

4.3 Thermal Hydraulic Analysis

Several thermal hydraulic design studies of breeding blankets (e.g., STARFIRE and INTOR) have been carried out based on a number of design concepts such as breeder in tube (BIT) and coolant in tube (CIT). One of the major uncertainties in these designs has been the thermophysical properties of the solid breeder, especially the thermal conductivity, which not only

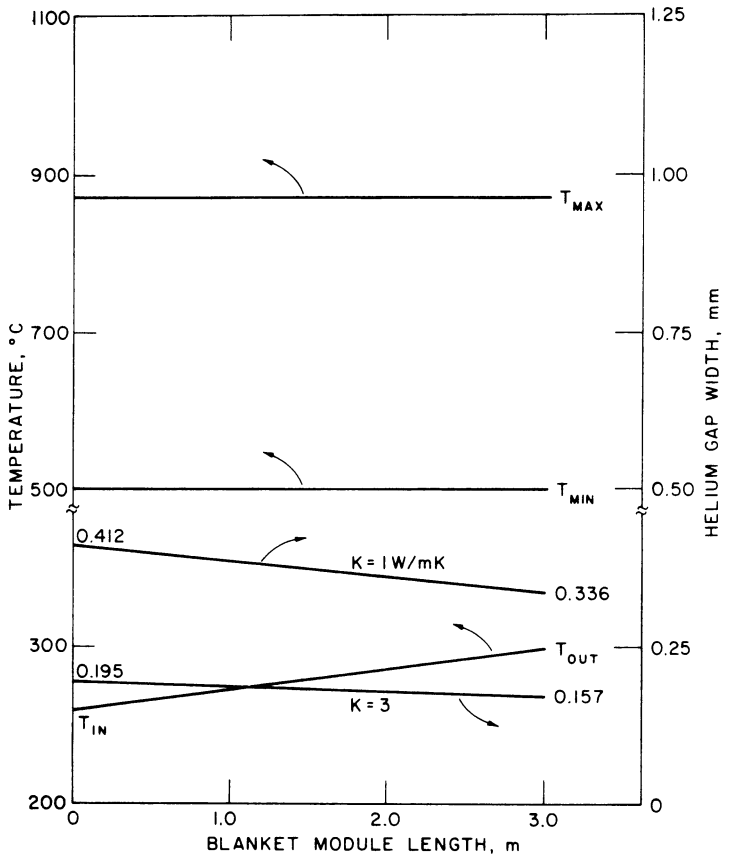

FIG.10
Coolant and blanket temperature distribution in blanket module, and helium gap as a function breeder thermal conductivity.

affect the blanket design but also the tritium breeding ratio and the tritium extraction rate. A parametric investigation was carried out covering a range of thermal conductivity (k) values (e.g., k varying from 3 W/mK for the best conducting solid breeders such as Li_2O to k = 1 W/mK for the poorer conducting solid breeders such as Li_2ZrO_3) to assess how the blanket design is influenced by the uncertainty in the thermal conductivity data. The uncertainties in available data for thermal conductivity were discussed in Sec. 4.1.

Figure 9 (CIT concept) schematically shows a breeder segment that was used for thermal hydraulics modeling. For a set

of parametric studies, the following design and operating conditions were assumed:

Coolant tube, i.d. (mm)	10
Coolant tube wall thickness (mm)	1.25
Breeder material	α-$LiAlO_2$
Breeder module length (m)	3.0
Coolant (H_2O) inlet temperature (°C)	260
Coolant outlet temperature (°C)	300
Minimum breeder temperature (°C)	500
Maximum breeder temperature (°C)	850
Nuclear heating in breeder (W/cc) (near first wall load = 1.3 MW/m^2)	15.9

The total tritium inventory in the solid breeder is the sum of diffusive inventory which is very sensitive to temperature distribution, and the solubility inventory. Hence, maintaining the proper temperature distribution in the solid breeder is one of the primary considerations for the blanket and lower temperature limits or the solid breeders have been selected based on such factors as thermal and irradiation-induced sintering, densification, pore restructuring, tritium diffusion, etc., which control tritium retention and release rates. The parametric investigations that were carried out during the STARFIRE design studies showed that the diffusive inventory of tritium can be very large even though only a small volume fraction (e.g., ~5%) of the breeder is below the lower temperature limit. Hence, it would be necessary to carry out the blanket design that leads to a breeder temperature distribution bounded by the temperature window, and thus minimize the tritium inventory. This temperature window varies from one breeder material to another. In this work, we consider 500-850°C which is typical of $LiAlO_2$.

The temperature distribution in a typical breeder segment is shown in Fig. 9, where (a) the temperature between 1-2 shows the temperature drop across the coolant film; (b) the temperature between 2-3 shows the wall temperature drop; (c) the temperature between 3-4 shows the temperature drop across the interfacial gap between the coolant tube wall and the breeder; and (d) the temperature drop between 4-5 shows the temperature gradient across the breeder. It can be shown that for the above set of operating conditions, the temperature window for the breeder cannot be maintained for the interfacial contact resistance that would normally be expected between the coolant tube and the ceramic breeder. Hence, it would be necessary to tailor the gap

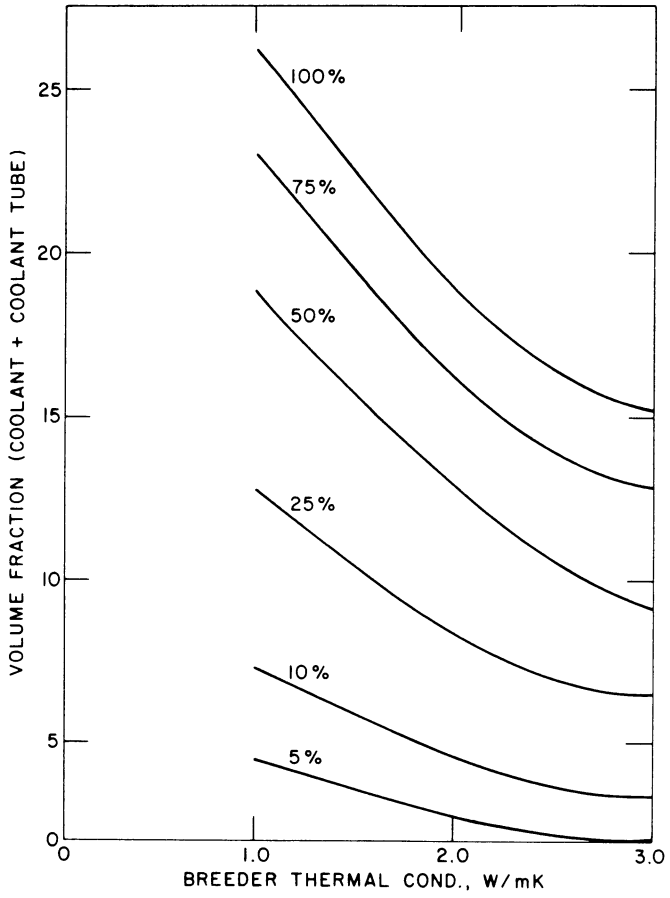

FIG.11
Volume fraction versus thermal conductivity.

conductance to obtain the desired temperature window (i.e., T_{min} = 500°C, T_{max} = 850° C). A ceramic insulator may be interposed between the coolant tube and the breeder to tailor the temperature distribution. Since the tritium retention capacity of the desired insulating material is not known, and since the thermal conductivity of most of the ceramic insulators is larger than that of an inert gas such as helium, doubled-walled coolant tubes with a helium-filled gap appears to offer some means of temperature control. Figure 10 shows the temperature distribution (based on the assumed operating conditions) along the coolant flow path and the helium gap thickness for two values of breeder thermal conductivity. The variation in the helium gas

thickness between the coolant inlet and the coolant outlet sections is due to the fact that the temperature drop across the gap at the coolant inlet must be 40°C higher than that of the coolant outlet (note: the coolant temperature rise across the blanket is 40°C).

An examination of the gap thickness corresponding to coolant inlet and the coolant outlet shows that the gap thickness variation is less than 100 μm over 3-m long coolant channels. While it is theoretically possible to produce double-walled tubes with controlled gaps, it may not be practical to maintain such gaps due to tube saging and manufacturing tolerances. It may be noted that if one were to maintain the same temperature window at every region in the blanket, the gap thickness must vary between the regions. This will further complicate the manufacture of double-walled tubes. In the analytical studies for STARFIRE, a fixed gap was used for all regions, and the tritium inventory calculations were based on resultant temperature distribution.

Based on the design and operating conditions, the volume fraction of the coolant plus the coolant tube structural material are plotted against breeder thermal conductivity for power factor values of 100%, 75%, 50%, 25%, 10% and 5% in Fig. 11. It can be seen from Fig. 11 that there is a maximum of 11% decrease in breeder volume at the first wall (i.e., at 100% region), and s value drops to ~2% at the rear of the blanket. This shows that when the thermal conductivity of the breeder is decreased from 3 W/mK to only 1 W/mK, the breeder volume is expected to decrease on the average of about 7%. Based on the results of the previous ANL studies [1], the reduction in the tritium breeding ratio due to the lower breeder volume is expected to be significant. It should be noted that the temperature distribution and the resultant tritium inventory considerations are based on limited data. More data, not only on the thermophysical properties of the solid breeders, but also on the tritium retention and release rates are needed to carry out the breeding blanket designs on a firmer basis. It is expected that the forthcoming TRIO-1 experiments will provide some of the critical design data.

4.4 Choice of Coolant

The most promising coolant types for fusion reactors are liquid metals, helium, and water. Liquid lithium offers unique advantages. It can simultaneously perform the functions of tritium production, heat deposition, and heat transport resulting in a simple low-pressure system. It is also compatible with most candidate structural materials. The major problem with

TABLE V. KEY AREAS OF COMPARISON BETWEEN HELIUM AND HELIUM AND WATER COOLANTS IN STARFIRE

1.	Gross thermal efficiency
2.	Pumping power requirements
3.	Inner blanket, shield thickness (void space with helium)
4.	Primary coolant loop plus stream enerator cost
5.	Outer blanket/shield thickness
	— Outer leg of the TF coil
	— Design of EF coils
6.	Shielding
	— Streaming through helium ducts
	— Crud in water loops
7.	Achievable tritium breeding ratio in solid breeders
8.	Ease of in-situ tritium recovery from solid breeders with narrow temperature range
9.	Chemical reactivity
10.	Coolant leakage
11.	Overpressure on reactor building
12.	Requirements for an intermediate coolant loop
13.	Cost of coolant and coolant purification (e.g. crud and tritium)

liquid lithium is the large stored chemical energy. The associated safety problems are of concern. Previous design studies and experience from the LMFBR program indicate that special design features, e.g. multiple barriers between liquid lithium and air and water, can reduce the probability of lithium fire to very low levels. However, these preventive design and operation measures are costly. Furthermore, liquid lithium has other disadvantages that include difficult problems in maintenance and cleanup of spills, a need for an intermediate coolant, and MHD effects. Therefore, it seems prudent at this stage of fusion research and development to seriously explore other options that offer potential for attractive safety features. It was in this spirit that a decision was made in the STARFIRE and DEMO studies to focus on solid breeders. Some effort was also devoted to studying the less-reactive liquid metals such as 17Li-83Pb.

TABLE VI. SUMMARY OF KEY POINTS IN THE WATER AND HELIUM COOLANTS COMPARISON FOR STARFIRE

	Water	Helium
Pressure, psi	2200	1500
Inner blanket/shield thickness, m	1.20	1.38
Maximum magnetic field, T	11.1	11.1
Maximum field on axis, T	5.80	5.52
Thermal power, MW	4000[a]	3305[a,b]
Coolant temperature, °C		
Reactor exit	320	475
Reactor inlet	280	300
Gross thermal efficiency, %	35.7	40
Coolant pumping power, MW	33	153
Other auxiliary power, MW	207	207
Net electric power,[c] MW	1200	1011
Cost of primary coolant loop	63	111
Direct plant capital cost, M$	1700	1620
$/kWe (relative units)	1.0	1.12

[a] Includes 200 MW in the limiter, which is removed by a separate water coolant.

[b] 621 MW of this power is deposited in the first wall and is removed by a water coolant.

[c] Account is made for the fact that the pmping power is added to the coolant as thermal energy; efficiency of helium circulator = 0.8.

The choice between helium and pressurized water for a solid breeder blanket involves a number of issues. Table V shows a large number of technical areas of the reactor design affected by the choice of one of these two coolants. A detailed comparative study of the two coolants was performed.

The primary advantage of helium cooling is a potentially higher thermal conversion efficiency than pressurized water. The reason for this is that a helium gas can be operated at high temperatures (e.g. 700-900°C) with reasonably low pressure (e.g. 5-8 MPa) while water requires higher pressures at low temperatures (critical temperature ~370°C). However, a key problem

that must be clearly recognized is that there is no structural material presently indentified that (a) can operate at temperatures >500°C; (b) is resistant to radiation damage; and (c) is compatible with impurities in helium. Modified austenitic stainless steel, PCA, is judged to be the only acceptable material with helium if no aggressive materials development program is pursued. This is a key assumption in this study since the maximum operating temperature of stainless steel is ~500°C, thus severely limiting the usefulness of helium. Under these conditions, and accounting for the larger pumping power requirement for helium, the net thermal conversion efficiency with helium is only a few percent higher than that for pressurized water.

All useful solid breeders that satisfy the tritium recovery, chemical, and radiation stability and material compatibility constraints were found to have a low tritium breeding potential and required placing a breeding blanket in the inboard region. This conclusion strongly impacts the helium/water comparison in view of the serious negative effect of void space in the inner blanket on tokamak reactor performance and economics. For the conditions of STARFIRE, the use of helium requires increasing the inboard/blanket/shield thickness by ~15-20%.

The capital cost of the primary coolant heat transport system (pipes, pumps, heat exchangers, etc.) is significantly larger with helium. Other difficulties with helium relate to radiation streaming through coolant manifolds, containment of helium, and the additional structural material requirements in the blanket.

Table VI shows a summary of the key points regarding the comparison of performance and economics for pressurized water and helium coolants for the STARFIRE conditions. The cost per unit power is shown to be significantly higher, ~13% with helium cooling. Therefore, pressurized water is a much better coolant than helium for tokamaks if the structural material temperature is limited to ~500°C. Furtheremore, using helium in the inboard blanket makes helium cooling a costly option.

5. ECONOMICS AND ENGINEERING

Cost estimates were carefully developed for STARFIRE and are detailed in Ref. [1]. In this section, an attempt is made to compare the cost of energy from tokamak power reactors to those of light-water reactors (LWR) and coal power plants. Furthermore, areas of uncertainties in the economics of future tokamaks are discussed.

TABLE VII. COMPONENTS OF COST OF GENERATING ELECTRICITY[a]

	Fusion[b] (%)	Fission[c] (%)	Coal[c] (%)
Capital	90	70	50
O&M	10	5	10
Fuel	0.01[d]	25	40

[a] All estimates are based on 1990 initial year of operation.

[b] Typical of several recent studies.

[c] Reference 28.

[d] Cost of deuterium and initial inventory of tritium. The cost of tritium recovery and reprocessing is included in the capital cost. In mature fusion power economy the cost of initial inventory of tritium is small (short doubling time reduces T cost dramatically).

The busbar electricity cost consists of three components: (1) the return on capital (fixed cost); (2) the operation and maintenance cost (O&M); and (3) cost of fuel. The percentage contribution of these three components varies substantially for the three energy options as shown in Table VII. In particular, the cost of fuel is negligible for a fusion power plant while it represents ~25% and 40% of the cost of electricity for LWR and coal, respectively. This is an extremely important point in view of the fact that trends of the past decade indicate that the cost of fuel experiences a much higher escalation rate than the cost of labor, materials, and construction.

Table VIII provides a comparison of the cost of electricity for three types of power plants: (a) fusion as represented by a STARFIRE-type tokamak; (b) LWR without reprocessing; and (c) coal. The assumptions employed are: (1) each power plant produces 1200 MW of net electtical power; (2) capacity factor = 0.65; (3) construction period is 6 y; (4) fixed charge rate = 17%; (5) escalation rate is 5% per year; and (6) initial year of operation is 1990. The cost estimates for coal and LWR are

TABLE VIII. COMPARISON OF COAL, FISSION, AND FUSION ECONOMICS

(1200 MWe Units, Initial Year of Operation 1990, Fixed Charge of 17%, Escalation Rate of 5%/y Capacity Factor of 65%)

	Fixed	O&M	Fuel	Total
A. Mills/kWh at Initial Year of Operation, 1990				
Fusion	66	7.8	0.2	74
Fission[a,b]	44	3.0	15.0	62
Coal	36	6.0	27.0	69
B. Mills/kWh at Mid-Life, Year 2005				
Fusion	66	16	0.4	82
Fission[a]	44	6	31	81
Coal[b]	36	13	55	104

[a]LWR without reprocessing.

[b]Reference for coal and fission: Ref. 28.

TABLE IX. ECONOMIC BENEFITS OF NEGLIGIBLE FUEL COSTS IN FUSION REACTORS

(Based on Fuel Escalation = 4% Above Inflation)

Initial Year of Operation	Fusion	Fission	Coal
1990	74	62	69
2000	74	69	82
2010	75	80	101
2020	75	96	129

taken from the detailed study of Ref. 28. The basic cost estimates for fusion are taken from STARFIRE [1]. As shown in Table VIII, the busbar energy cost for the initial year of operation (1990) is 74, 62, and 69 mill/kWh for fusion, fission, and coal, respectively. The fusion cost is the highest for the initial year of operation and it also has the largest uncertainty. However, if one assumes that the fuel cost will escalate at an additional 4%/y above inflation, the economic picture changes. The lower portion (B) of Table VIII shows the cost of energy at the year 2005, i.e. at midlife, for the same plants in the upper portion (A; initial operation 1990). The cost of energy in this case is roughly the same for fusion and fission; and both are significantly lower than for coal. Following standard economic practices, one finds that the levelized (or simply the normalized average over 30-y life) cost of energy for STARFIRE-type tokamaks is comparable to that of future LWR'S and significantly lower than that for coal power plants. Table IX shows the cost of energy during the initial year of operation for plants starting in the years 1990, 2000, 2010, and 2020. These results show a favorable economic trend for fusion reactors. The picture becomes even more favorable to fusion when the levelized cost of energy is estimated for the 30-y life of each plant.

The key issue in the economic comparison given above concerns the uncertainties in the cost estimates for fusion. Notes on these uncertainties are given below.

The cost of energy is directly proportional to the capital cost and inversely proportional to the plant availablity factor. The capital cost estimates for STARFIRE are the most comprehensive estimates made to date for a fusion reactor. Confidence in these estimates is enhanced by the details in the definition of the reference design and by the use of an extensive data base for costing materials and labor. Furthermore, roughly one-half of the direct capital cost is attributable to the balance-of-plant, for which most of the cost estimates are based on direct quotes from manufacturers.

The greatest uncertainties in the economics of future tokamak power plants concern the plant availability factor. This is crucially dependent on component lifetime and reliability (low frequency of component failure) and maintainability (short downtime to replace failed components). The data base for the lifetime and reliabilty of components in the fusion reactor environment is lacking, and such information must be obtained as a part of the technology development program. Definitive information on reactor maintainability will come only from experience with cooperation and maintenance of future fusion devices. In the

meantime, every effort must be taken to incorporate design features and select design and technology options that enhance the probability of a reasonably high availability factor.

The STARFIRE design attempted to maximize component and reactor reliability and maintainability. Component lifetime and reliability are enhanced by the choice of steady-state mode of operation; by locating, whenever feasible, key components (e.g., poloidal coils, vacuum pumps) away from the harsh radiaton environment; and by developing a design in which the engineering burden is optimally shared among reactor components (e.g., radiating the alpha power from the plasma to the first wall in order to reduce the heat load on the particle-collection medium to a manageable level). Special attention was given to maximizing the reliability of components that are difficult to replace. For example, conservative design margins were incorporated into the design of the TF coils since their replacement requires long downtimes.

Simplying the reactor design has been a key approach in STARFIRE to enhancing component reliability and maintainability. The choices of the noninductive current driver and the limiter/vacuum system concept have contributed significantly to simplifying STARFIRE. Other features found important in enhancing reactor maintainability include: modularity; locating the vacuum boundary at the shield with all mechanical seals; placing all service connenctions outside the vacuum boundary; and locating all superconducting EF coils outside the TF coils. A relatively low number, 12, of TF coils was used to increase accessibility. There remains a great incentive for further reducing the number of TF coils. Therefore, more accurate information on the allowable field ripple in reactor-size plasmas is needed. The STARFIRE maintenance plan calls for a "remove and replace" approach; i.e., the failed components are replaced with standby units and the reactor is operated while the failed parts are repaired in the hot cell. This approach seems necessary in order to achieve reasonable availability goals.

ACKNOWLEDGMENT

We wish to thank D. Mikkelsen for calculating the neutral beam-driven current for the DEMO reactor.

REFERENCES

[1] BAKER, C.C., et al, STARFIRE, A Commercial Tokamak Fusion Power Plant Study, Argonne National Laboratory Rep. ANL/FPP-80-1 (1980).

[2] A Demonstration Power Plant Study, Argonne National Laboratory Rep., to be issued (1982).
[3] YAMAMOTO, T., et al., Phys. Rev. Lett. 45 (1980) 716.
[4] FUKUDA, M., MATSUURA, K., J. Phys. Soc. Japan 44 (1978) 1344.
[5] YOSHIKAWA, S., YAMATO, H., Phys. Fluids 9 (1966) 1814.
[6] START, D.F.H., et al., Phys. Rev. Lett. 40 (1978) 1497.
[7] MOHRI, A., et al., Plasma Physics and Controlled Nuclear Fusion Research (Proc. 7th Int. Conf., Innsbruck, 1978) Vol. 3, IAEA, Vienna, 311.
[8] FISCH, N.J., KARNEY, C.F.F., Phys. Fluids 24 (1981) 27; KARNEY, C.F.F., FISCH, N.J., Phys. Fluids 22 (1979) 1817; FISCH, N.J., BOOZER, A.H., Phys. Rev. Lett. 45 (1980) 720; FISCH, N.J., Nucl. Fusion 21 (1981) 15.
[9] EHST, D.A., J. Fusion Energy (to be published); see also EHST, D.A., Wave-Driver Options for Low Aspect Ratio Steady-State Tokamak Reactors, Argonne National Laboratory Rep. ANL/FPP/TM-141 (1981).
[10] GRISHAM, L.R., et al., Plasma Heating with Multi-MeV Neutral Impurity Beams, Princeton Plasma Physics Laboratorty Rep. PPPL-1759 (1981).
[11] EHST, D.A., et al., Bull. Am. Phys. Soc. 26 (1981) 965.
[12] BOLEY, C.D., BROOKS, J.N., "Study of plasma edge conditions for a commercial tokamak reactor," Engineering Problems of Fusion Research (Proc. 9th Symp., Chicago, 1981), to be published.
[13] FLANAGAN, C.A., et al. Initial Grade and Design Studies for the Fusion Engineering Device, Oak Ridge National Laboratory Rep. ORNL/TM-7777, to be published.
[14] BROOKS, J.N., MC GRATH, R., "Redeposition of the sputtered surface in lmiters," Engineering Problems of Fusion Research (Proc. 9th Symp., Chicago, 1981) to be published.
[15] ABDOU, M., "Divertor collector plate and channel," The U.S. Contribution to the International Tokamak Reactor Phase-I Workshop - Conceptual Design, INTOR/81/1 (1981), Chapt. VIII.
[16] MATTAS, R., et al., "Materials selection for the U.S. divertor collector plate," Fusion Reactor Materials (Proc. 2nd Top. Mtg., Seattle, 1981) to be issued.
[17] SMITH, D., et al., Fusion Reactor Blanket/Shield Design Study, Argonne National Laboratory Rep. ANL/FPP-79-1 (1979), 6-34, 6-35.
[18] ARONS, R.M., et al., "Preparation, characterization, and chemistry of solid ceramic breeder materials," Fusion Reactor Materials (Proc. 2nd Top. Mtg., Seattle, WA, 1981) to be issued.
[19] SUITER, D., DAVIS, J.W., "Development of solid tritium breeding compounds for use in fusion reactors," ibid.

[20] HOLLENBERG, G.W., Hanford Engineering Development Laboratory, personal communication (1981).
[21] FINN, P.A., Argonne National Laboratory, personal communication (1981).
[22) TANIFUGIS, T., SHIOZANA, K., NASU, S., J. Nucl. Mater. 78 (1978) 422-424.
[23] NASU, S., TANIFUGI, T., TAKESHITA, H., Comments on the tritium solubility of Li_2O as a solid tritium-breeding material, Nucl. Sci. Eng., to be issued.
[24] JOHNSON, A.B., KABELE, T.J., GURWELL, W.E., Tritium Production from Ceramic Targets, Battlle Pacific Northwest Laboratory Rep. BNWL-2097 (1976).
[25] CHAPRA, O.K., SMITH. D.L., "Interactions of solid ceramic breeding materials with structural alloys," Fusion Reactor Materials (Proc. 2nd Top. Mtg., Seattle, 1981) to be issued.
[26] FINN, P.A., BREON, S.R., CHELLEW, N.R., "Compatibility study of solid ceramic breeder materials," ibid.
[27] FINN, P.A., Argonne National Laboratory, personal communication (1981).
[28] ROBERTS, J.O., et al., Coal and Nuclear: A Comparison of the Cost of Generating Baseload Electicity by Region, NRC Document NUREG-0480 (1978).

Printed by the IAEA in Austria